JACS
JOURNAL OF THE AMERICAN CHEMICAL SOCIETY

ARTICLE

pubs.acs.org/JACS

Fluorescence Microscopy of the Pressure-Dependent Structure of Lipid Bilayers Suspended across Conical Nanopores

Anna E. P. Schibel, Emily C. Heider, Joel M. Harris,* and Henry S. White*

Department of Chemistry, University of Utah, 315 South 1400 East, Salt Lake City, Utah 84112, United States

Supporting Information

ABSTRACT: Glass and fused-quartz nanopore membranes containing a single conically shaped pore are promising solid supports for lipid bilayer ion-channel recordings due to the high inherent stability of lipid bilayers suspended across the nanopore orifice, as well as the favorable electrical properties of glass and fused quartz. Fluorescence microscopy is used here to investigate the structure of the suspended lipid bilayer as a function of the pressure applied across a fused-quartz nanopore membrane. When a positive pressure is applied across the bilayer, from the nanopore interior relative to the exterior bulk solution, insertion or reconstitution of operative ion channels (e.g., α-hemolysin (α-HL) and gramicidin) in the bilayer is observed; conversely, reversing the direction of the applied pressure results in loss of all channel activity, although the bilayer remains intact. The dependence of the bilayer structure on pressure was explored by imaging the fluorescence intensity from Nile red dye doped into suspended 1,2-diphytanoyl-*sn*-glycero-3-phosphocholine bilayers, while simultaneously recording the activity of an α-HL channel. The fluorescence images suggest that a positive pressure results in compression of the bilayer leaflets and an increase in the bilayer curvature, making it suitable for ion-channel formation and activity. At negative pressure, the fluorescence images are consistent with separation of the lipid leaflets, resulting in the observed loss of the ion-channel activity. The fluorescence data indicate that the changes in the pressure-induced bilayer structure are reversible, consistent with the ability to repeatedly switch the ion-channel activity on and off by applying positive and negative pressures, respectively.

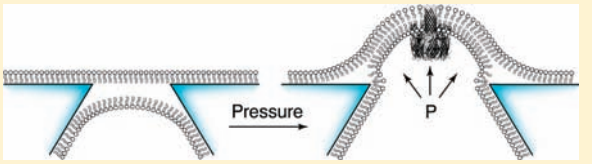

INTRODUCTION

Ion-channel recordings have gained much attention in recent years for single-molecule detection, drug screening, and DNA sequencing, in addition to traditional investigations of fundamental biophysical phenomena.[1−15] Consequently, focus has been brought to the development of solid supports for suspended lipid bilayer membranes. In recent reports, we have described the fabrication and application of glass and fused-quartz nanopore membranes (GNM and QNM, respectively) for ion-channel recordings.[16−21] The GNM/QNM contains a single, conically shaped nanopore embedded within an ∼50-μm-thick glass or fused-quartz membrane at the end of a glass or fused-quartz capillary.[18,21] A lipid bilayer can be suspended across the orifice following modification of the glass or quartz surface with (3-cyanopropyl)dimethylchlorosilane to impart an intermediate hydrophobic surface character. The assumed structure of the lipid bilayer membrane across the nanopore orifice is presented in Figure 1A. Suspended lipid bilayers on GNMs and QNMs display exceptional stability and long lifetimes due to the reduced area of the bilayer (∼1 μm^2 for a typical 500-nm-radius nanopore orifice).[20−22] In addition, the reduced bilayer area minimizes the bilayer capacitance, which can limit high-frequency data acquisition.

Ion-channel activity using GNMs and QNMs is observed only with the application of a small positive pressure (20−300 mmHg) across the membrane, from the nanopore interior relative to the exterior bulk solution, and is observed as a discrete increase in current due to protein reconstitution within the bilayer (α-HL has a conductance of ∼1 nS in 1 M KCl[23]). This activity can be reversed by removing the pressure or by applying a small negative pressure.[20] The pressure-controlled channel activity is observed regardless of whether the protein is in the solution inside the capillary or in the external bulk solution, and it can be repeatedly turned on and off as the applied pressure is varied between positive and negative pressures, respectively. Figure 1B shows an example current−time (i−t) trace of α-hemolysin (α-HL) ion-channel activity as a function of applied pressure. This unique ability to control ion-channel activity indicates a dynamic pressure-dependent bilayer structure. To our knowledge, the nanopore membrane is the only ion-channel support for which pressure can be used to reversibly control ion-channel activity.

When a solution of lipid molecules dispersed in an organic solvent is spread across a large circular opening (≥50 μm radius) in a hydrophobic solid membrane, e.g., Teflon, that is immersed in an aqueous solution, a lipid bilayer will spontaneously form across the opening as a means to reach the lowest free energy state.[24] This suspended bilayer structure is described as possessing a region of bulk lipid solution around the perimeter of the lipid bilayer, adjacent to the walls of the circular opening, which is defined as the annulus, torus, or Plateau−Gibbs border.[25−28] The annulus region contains organic solvent and excess lipid

Received: December 29, 2010
Published: May 04, 2011

dx.doi.org/10.1021/ja1117182 | *J. Am. Chem. Soc.* 2011, 133, 7810–7815

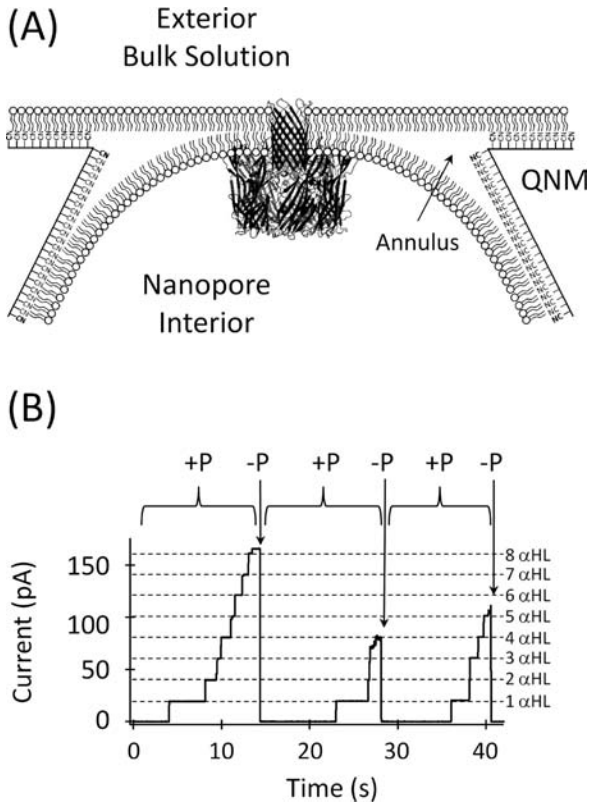

Figure 1. (A) Cross-sectional schematic (not drawn to scale) of an α-HL pore embedded in a bilayer suspended across the orifice of a QNM. (B) Example $i-t$ trace showing the pressure-controlled α-HL activity in a solution containing 1 M KCl, 30 mM Tris-HCl, 10 mM EDTA (pH 7.4), and 3 μM α-HL. The step increases in current correspond to individual α-HL pores when a positive pressure, $+P$, of 50 mmHg (*internal nanopore solution* vs *external solution*) is applied across the lipid bilayer; α-HL pore activity disappears when the pressure is either removed or reversed ($-P$). $i-t$ data were collected at an applied voltage of 30 mV (*internal* vs *external*).

molecules, which are organized into inverse micelles.[28] The bilayer is suspended across the orifice and is connected to the solid support via the annulus. The spontaneous thinning of the lipid solution into a lipid bilayer is due to (i) the curvature-induced pressure-driven flow of the bulk lipid solution into the Plateau−Gibbs border, (ii) van der Waals interactions between the aqueous phases separated by the bilayer, and (iii) van der Waals interactions between the hydrocarbon chains of the lipid molecules.[25−28]Additionally, when a voltage is applied across the lipid structure, the electric field aids in thinning.[26−28]

The orifice cross-sectional areas of GNMs and QNMs are ∼2−3 orders of magnitude smaller than in the traditional devices (Teflon membranes, Delrin cups, etc.) used for investigating the annulus region and mechanism of bilayer thinning. The larger orifices in these polymer membranes will have a smaller volume of lipid solution relative to the orifice dimensions, in comparison with GNM/QNMs; thus, the smaller size of GNM/QNMs may inhibit the lipid solution from spontaneously thinning across the orifice. If the lipid solution does not thin into a bilayer, ion-channel reconstitution or activity will not occur. We observe that an external pressure force is required for observing ion-channel activity using GNM/QNMs, suggesting a fundamental difference in the bilayer structure suspended across large and small orifices.

Fluorescence imaging has been shown to be useful in characterizing the nature of artificial bilayers,[29−31] and imaging techniques have previously been successfully combined with electrical recordings to simultaneously monitor ion-channel activity.[32−34] Here, epi-illumination fluorescence microscopy is used to observe the structure of lipid bilayers suspended across the orifice of a QNM, as a function of applied pressure. Nile red fluorescent dye is dissolved in the lipid solution (1,2-diphytanoyl-*sn*-glycero-3-phosphocholine in decane) used to form a bilayer. The resulting bilayer is imaged as a function of applied pressure while simultaneously recording the α-HL ion-channel activity. To avoid fluorescent artifacts from the glass in GNMs, nanopore membranes prepared from fused-quartz capillaries are used. QNMs possess surface properties and ion-channel reconstitution capabilities similar to those of GNMs, in addition to improved electrical and optical properties.[21,35] It is found that the bilayer structure and lipid solution distribution at conically shaped pores varies as a function of pressure. Due to the asymmetric pore geometry, a thinning and protrusion of the bilayer (which allows for ion-channel reconstitution) occurs with positive pressure, and a withdrawal of the lipid solution into the pore occurs with negative pressure. The fluorescence images are consistent with the dependence of ion-channel activity on applied pressure.

EXPERIMENT

Materials. Aqueous solutions were prepared using 18 MΩ·cm water obtained from a Barnstead E-pure water purifier. KCl, K_2HPO_4, KH_2PO_4, and EDTA were used as received from Mallinckrodt to prepare buffered electrolyte solutions (containing either 1 M KCl, 10 mM PBS, and 1 mM EDTA (pH 7.4), or 1 M KCl, 30 mM Tris-HCl, and 10 mM EDTA (pH 7.4)). (3-Cyanopropyl)dimethylchlorosilane was used as received from Gelest. Decane was obtained from Fisher Scientific, and 1,2-diphytanoyl-*sn*-glycero-3-phosphocholine (DPhPC) was obtained from Avanti Polar Lipids in 10 mg aliquots dispersed in chloroform. Nile red dye was purchased from Invitrogen (Cat. No. N-1142) as a powder, dispersed in chloroform (spectroscopy/LC grade, from Omnisolve), and stored at −4 °C at a concentration 0.5 mg/mL when not in use. α-HL monomer was obtained from Sigma-Aldrich as a lyophilized powder, stored at 0.6 mg/mL in H_2O in a −80 °C freezer, and diluted to ∼240 nM with buffered electrolyte upon thawing. α-HL solutions were stored in a refrigerator (4 °C) for short periods of time between experiments. Glass coverslides (No. 1, 22 × 22 mm) were obtained from VWR and used to form the base of a well when attached to a glass cylinder via epoxy. This well was used as the experimental cell for simultaneously recording ion-channel activity and fluorescence images. Ag wire for Ag/AgCl electrodes was purchased from Alpha Aesar (0.25 mm and 0.5 mm diameter).

QNM Fabrication. The fabrication of the QNM has been previously reported[21] and is only briefly described here. A 50-μm-radius tungsten wire is attached to a tungsten rod via silver conductive adhesive paste; the end of the wire is then electrochemically sharpened in 1.5 M NaOH while applying 10 V_{PP} at 60 Hz. The nanopore membrane is formed by initially sealing the end of a 3−4-cm length of fused-quartz capillary with a H_2/O_2 flame. Once the fused-quartz membrane is formed, the sharpened W wire is inserted into the capillary and positioned within 15 μm of the membrane. The quartz is then heated again in the H_2/O_2 flame while applying a vacuum to the end of the capillary, collapsing the fused-quartz membrane until the W wire is sealed into the membrane. The sealed end of the capillary is polished, leaving a thin fused-quartz membrane (25−75 μM thick) in which a W disk is exposed. Finally, the W wire is partially etched out of the orifice in a

1.5 M NaOH solution by applying 10 V_{PP} at 60 Hz; the remaining wire is manually removed by pulling the W rod out of the capillary. The approximate size of the W disk is monitored during polishing with an electrical feedback circuit which indicates when the desired radius has been reached. The radius of the nanopore orifice is determined from the measured conductance in 1 M KCl.[18−20] The fused-quartz surface is chemically modified with (3-cyanopropyl)dimethylchlorosilane in order to create the hydrophobic surface character required for formation of the suspended bilayer structure.[19,20]

Ion-Channel Recording. The QNM was filled with buffered electrolyte containing 240 nM α-HL and submerged in a cell containing the same electrolyte (without α-HL). Ag/AgCl electrodes (fabricated by immersing a Ag wire in Clorox bleach for 10 min) were used to apply a voltage bias (+40 mV, *internal* vs *external*) across the QNM. One Ag/AgCl electrode (0.25 mm diameter) was placed inside the QNM capillary, and the second (0.5 mm diameter) was placed in the external cell. The back of the QNM was sealed with a Dagan Corp. pipet holder attached to a pressure line and syringe; positive and negative pressures were applied by compression and release of the syringe plunger, respectively, and measured using a sphygmomanometer pressure gauge. A voltage was applied across the QNM with a Dagan Corp. CHEM-CLMAP (voltammeter and amperometer voltage clamp amplifier) interfaced with a PC, and the current was monitored.

To prepare the lipid for bilayer formation, a nitrogen stream was used to dry the chloroform from the DPhPC solution, and the lipid was redispersed in 1 mL of decane. Nile red dye was then added to the lipid solution at a concentration of 0.001% (by mass) in 10 mg of DPhPC per mL of decane. The 0.001% Nile red lipid solution was painted across the QNM orifice with a pipet tip while an $i-t$ trace was recorded. A decrease in conductance to ∼10 pS (corresponding to an ∼100 GΩ bilayer seal) indicates that a bilayer has formed.[20] Positive pressure was applied to the back of the QNM until α-HL insertion was observed, and then negative pressure was used to remove the α-HL activity. While monitoring α-HL activity through the $i-t$ trace, fluorescence microscopy was used to image the bilayer as a function of applied pressure. Protein channel activity was used to verify the presence of a functional bilayer; only bilayers that exhibited protein channel conductance of ∼1 nS in 1 M KCl were imaged. Figure 2 shows a depiction of the experimental setup.

Fluorescence Microscopy. Fluorescence images of the bilayer suspended across the QNM were captured with an inverted epi-illumination fluorescence microscope. The beam from a Lexel model 95 argon ion laser, tuned to 488 nm, was passed through a Pellin-Broca prism and selectively blocked with an electronic Uniblitz shutter to minimize sample photobleaching. The beam was scattered with a rotating, roughened glass disc to average the illumination speckle pattern. A 55-mm focal length lens (f/1.2) was used to reimage the scattered laser spot through the objective. A band-pass excitation filter (D480/30, Chroma) and a long-pass dichroic beam splitter (505dclp, Chroma) were placed before the objective (Nikon Plan Fluor 100×, 1.3 NA). The fluorescence emitted from the sample was collected by the same objective and separated from the excitation light via the dichroic beam splitter and a 510-nm long-pass emission filter (HQ510lp, Chroma); the depth of field was 1 μm. The fluorescence image was acquired with a Photometrics CoolSNAP HQ CCD detector (1392 × 1040 imaging array with 6.45 × 6.45 μm pixels).

Once a bilayer was formed, the position of the QNM was adjusted above the microscope stage using a micropositioner to bring the QNM surface into the focus of the objective. Images were captured with the focus of the objective at varying depths, as indicated in Figure 2: (i) at the external QNM surface ($z = 0$), (ii) above the external surface ($+z$) into the bulk solution, and (iii) below the external surface ($-z$) into the nanopore interior. The objective was adjusted in the z-direction by ±2 μm increments to image the Nile red distribution as a function of applied pressure. Each fluorescence image was acquired with a 1.0 s integration time.

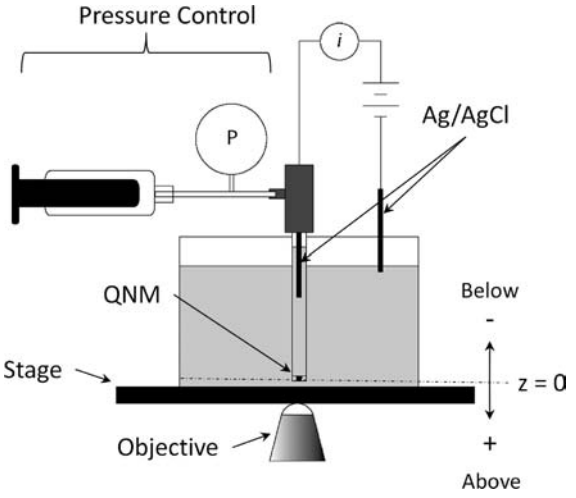

Figure 2. Schematic depiction of the experimental system for measuring the fluorescence intensity from the QNM-suspended bilayer as a function of applied pressure, while simultaneously performing ion-channel recordings. The QNM with a suspended DPhPC bilayer is submerged in a cell positioned on the stage of an inverted epi-illumination fluorescence microscope, while $i-t$ data are simultaneously recorded in a solution containing 1 M KCl, 10 mM PBS, 1 mM EDTA (pH 7.4). The internal volume of the QNM capillary contained 240 nM α-HL dissolved in the same solution and is connected to a gastight syringe for pressure control. The QNM surface is moved in the $\pm z$ direction relative to the microscope objective by moving the optical stage. In the experiments described below, $z = 0$ corresponds to the QNM exterior surface being located at the microscope focal point, while positions below (nanopore interior) and above (exterior bulk solution) the QNM surface are indicated as $-z$ and $+z$, respectively.

RESULTS AND DISCUSSION

Nile red is a hydrophobic dye, and, when dissolved in a hydrophobic environment[36,37] such as the acyl chain region of a lipid membrane[38,39] or a decane/lipid solution, its fluorescent emission is readily detectable. Nile red is very sensitive to the hydrophobicity of its environment;[40−42] it fluoresces strongly in a lipid/decane solution and is weakly emitting when dissolved in aqueous solution.[43] Thus, the fluorescence signal from Nile red was used to image the distribution of the lipid/decane at the QNM surface as a function of the applied pressure. Line scans of fluorescence intensity over the pore face and nanopore orifice were plotted to quantitatively assess the pressure-dependent bilayer structure. In these experiments, QNMs with orifice radii (1.5−2 μm) slightly larger than those previously employed in ion-channel recordings (0.5−1 μm) were used in order to observe structural features in the fluorescence images. The pressure-dependent activity of α-HL with these larger QNMs, however, is qualitatively similar to that previously reported.[20]

Figure 3 demonstrates how the fluorescence intensity varies across the QNM surface as a function of applied pressure. In this experiment, the QNM surface is brought into the focal plane of the microscope ($z = 0$), and a positive pressure (80 mmHg) is applied across the membrane (internal vs external solution). Beginning at ∼600 s in the $i-t$ trace, an α-HL channel is reconstituted in the bilayer, yielding a conductance of ∼1 nS (40 pA at V_{app} = 40 mV), in agreement with literature values in 1.0 M KCl.[22] The $i-t$ traces were recorded with an open cell, without a Faraday cage, in order to simultaneously record the fluorescence images, resulting in electrical noise larger than

dx.doi.org/10.1021/ja1117182 |J. Am. Chem. Soc. 2011, 133, 7810–7815

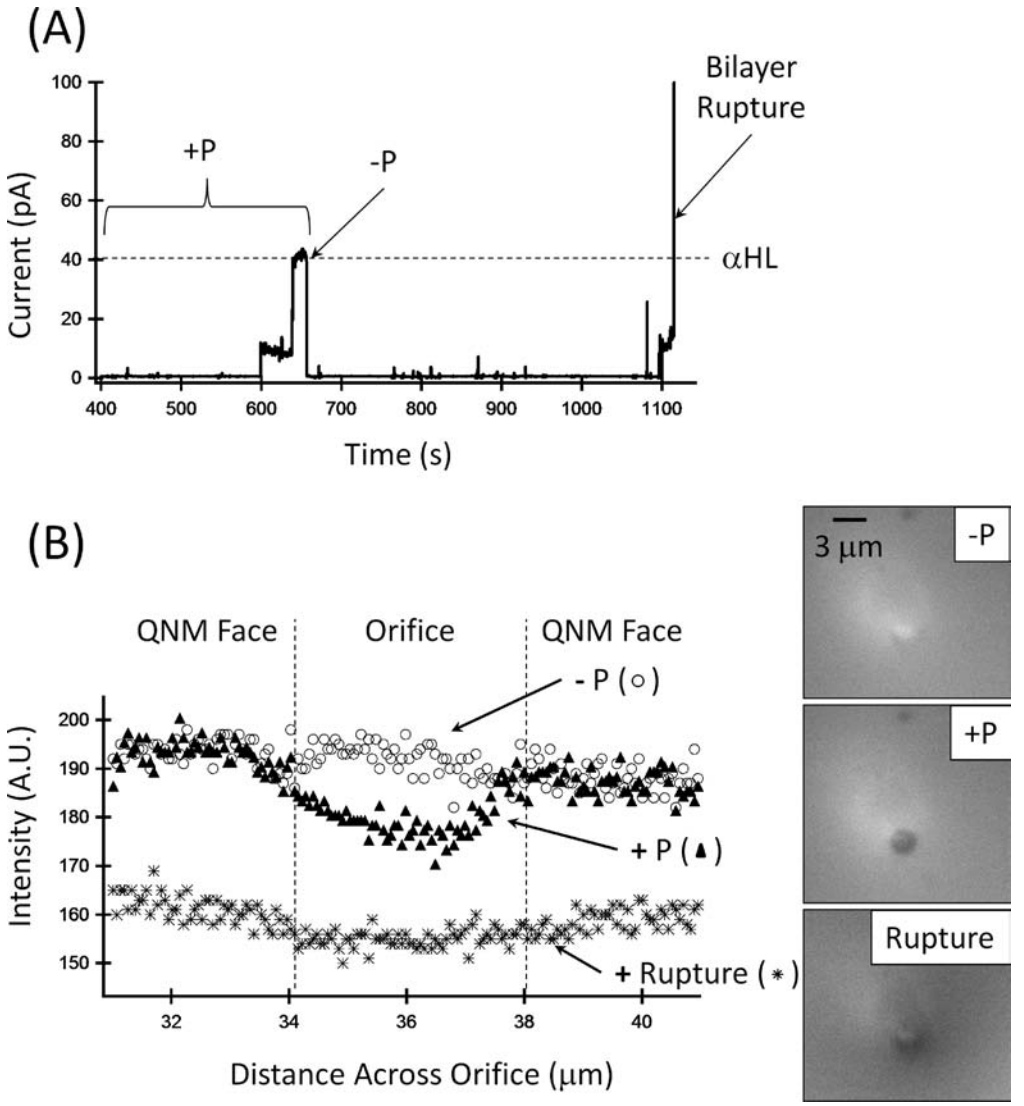

Figure 3. (A) $i-t$ trace showing the reconstitution of a single α-HL channel in a DPhPC bilayer suspended across the ~2-μm-radius orifice of a QNM. The solution conditions are the same as in Figure 2, and the $i-t$ trace was obtained at a voltage of 40 mV. $+P$ corresponds to +80 mmHg (internal vs external solution), while $-P$ corresponds to −20 mmHg. The bilayer was ruptured by applying 120 mmHg. (B) Fluorescence images and intensity line scans of the QNM/DPhPC bilayer were taken at ~650 ($+P$), ~690 ($-P$), and ~1130 s (bilayer rupture) during the ion-channel recording. The dashed horizontal lines correspond approximately to the orifice circumference, with the center of the orifice located at ~36 μm.

usually present in the α-HL channel recordings using glass nanopores.[22]

The fluorescence image obtained at positive pressure showed a decrease of fluorescence intensity over the pore orifice. Application of a negative pressure resulted in the immediate loss of α-HL activity and an increase in the fluorescence intensity across the pore orifice (relative to positive pressure). Upon bilayer rupture at a higher pressure (100 mmHg), the fluorescence intensity decreased across the nanopore membrane surface. Although the absolute fluorescence intensity and background signal vary using different QNMs and bilayers, the relative change in fluorescence intensity over the pore orifice as a function of applied pressure is reproducible. A positive pressure applied from the internal solution results in a decrease in fluorescence intensity across the pore orifice, where the lipid bilayer is located.

Pressure-dependent changes in the fluorescence intensity across the pore orifice were investigated as a function of the objective focus depth, as shown in Figure 4 (see the Supporting Information for the corresponding $i-t$ trace). Upon protein channel insertion with positive pressure, fluorescence images were acquired above the external surface ($z > 0$, see Figure 2), at the external pore surface ($z = 0$), and below the external surface ($z < 0$). A negative pressure was applied, and images were again recorded above the external surface, at the external pore surface, and below the external surface. Acquisition of the images was repeated again once the bilayer was ruptured. Fluorescence images are shown in Figure 4A as a function of the objective focus depth (at $z = +4$, 0, or −4), while Figure 4B plots the line scans of the fluorescence intensity over the pore face as a function of the objective focus depth ($z = +6$ to $z = -6$). Figure 4C depicts the lipid/decane structure as interpreted from the results presented in Figure 4A,B.

Figure 4A,B (left) summarizes the results of a series of fluorescence images for 60 mmHg applied pressure (nanopore interior

dx.doi.org/10.1021/ja1117182 |J. Am. Chem. Soc. 2011, 133, 7810–7815

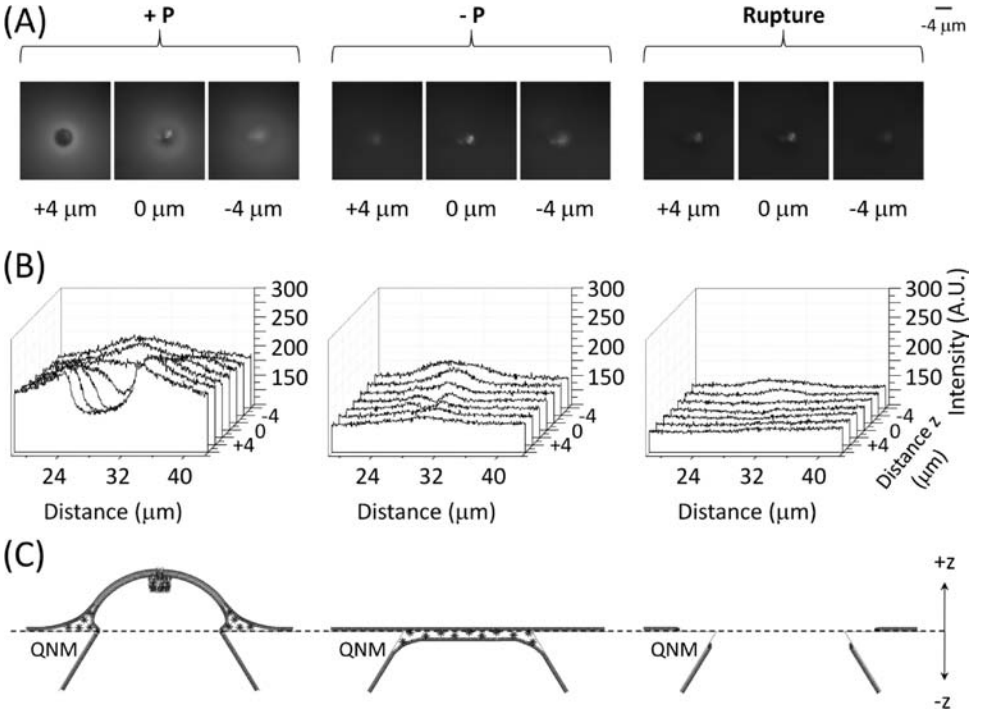

Figure 4. (A) Fluorescence images of QNM DPhPC bilayer with the microscope objective focus above the external QNM external surface ($z = +4\,\mu$m), at the external surface ($z = 0$), and below the external surface ($z = -4\,\mu$m) as a function of pressure left to right: $+P$ (+60 mmHg), $-P$ (−20 mmHg), and after bilayer rupture. (B) Fluorescence intensity line scans recorded for $+6 < z < -6$ at 2-μm increments at +60 and −20 mmHg and after bilayer rupture. (C) Schematic representation of the bilayer structure as interpreted from the fluorescence microscopy data. The corresponding $i-t$ trace can be found in the Supporting Information.

relative to the exterior bulk solution). The fluorescence images (Figure 4A) and line scans (Figure 4B) show the lipid distribution from $-6\,\mu$m below the external surface, at the pore face (0 μm), to $+6\,\mu$m above the external surface. At the pore surface (0 μm), there is a decrease in fluorescence intensity across the orifice and on the surface around the orifice. Above the external surface ($+4\,\mu$m), there is a ring of fluorescence brighter than at the QNM orifice and a decrease in fluorescence within the center. This configuration corresponds to conditions favorable for α-HL reconstitution and suggests a structure where the lipid solution is forced outside of and away from the orifice, resulting in a convex bilayer structure; i.e., the lipid/decane membrane has thinned to a bilayer capable of supporting an operative α-HL channel (Figure 4C, left). This hypothesis is further supported by previous observations that a pressure gradient induces curvature to the bilayer.[44−46] Images obtained below the external surface ($-4\,\mu$m) show that there is fluorescence concentrated across the orifice; this is attributed to lipid and decane collecting within the orifice and scattered fluorescence from the pore walls.

Figure 4A,B (center) summarizes the results at a negative applied pressure at various objective focus depths. When negative pressure is applied to the QNM, the fluorescence intensity decreases across the surface of the pore and increases across the pore orifice relative to the surrounding surface. This is the case both above the external surface (up to $+6\,\mu$m) and at the pore surface (0 μm); again, the fluorescence observed when the focus of the objective is below the external surface (up to $-6\,\mu$m) is postulated to be from lipid and decane within the orifice and scattered fluorescence from the pore walls. The microscope objective has a depth of field of ~1 μm and will collect out-of-focus fluorescence as well. However, the increase in fluorescence intensity across the pore orifice relative to the pore surface can be compared with images obtained at positive pressure where the intensity on the surface is greater than that across the orifice. The fluorescence distribution upon applying negative pressure suggests that dye (and thus lipid and decane) is accumulating within the orifice. These results are interpreted as the lipid/decane solution being pulled into the pore and thickening of the solution layer across the orifice as the bilayer leaflets are separated (Figure 4C, center). This conclusion is consistent with the observation that smaller orifice dimensions reduce the rate of spontaneous thinning of the lipid/solvent solution across the orifice.[47] Negative or zero pressure allows the lipid and decane to distribute within the pore and along the capillary walls, whereas positive pressure forces the lipid out from the pore, thinning the solution to the limit of a functional lipid bilayer.

Finally, Figure 4A,B (right) summarizes the fluorescence data following the rupture of the bilayer at high pressure. When the bilayer is ruptured, there is a decrease in fluorescence over the surface and within the pore, as seen from the intensity decrease compared with the positive and negative pressure images and line scans. These results are interpreted as an irreversible loss of the lipid and dye from the orifice region (Figure 4C, right).

CONCLUSIONS

Fluorescence microscopy images obtained during ion-channel recordings indicate that applying a positive pressure across the QNM results in a redistribution of the decane/lipid solution favorable for bilayer formation and ion-channel activity. The fluorescence images suggest that positive pressures push the decane/lipid solution outward from the orifice (toward the

dx.doi.org/10.1021/ja1117182 |J. Am. Chem. Soc. 2011, 133, 7810–7815

external solution), creating a convex lipid bilayer structure suitable for ion-channel reconstitution. Removal of this positive pressure (either zero or negative applied pressure) results in loss of ion-channel activity, a consequence of the decane/lipid solution being drawn into the orifice, as indicated by the increased fluorescence in the orifice region. Most likely, this flow results from surface tension pulling the decane/lipid solution into the pore. The loss of ion-channel activity after removal of the external postive pressure suggests that the lipid bilayer structure is unstable as the decane/lipid solution is drawn through the orifice of the pore.

■ ASSOCIATED CONTENT

Supporting Information. Current−time trace of α-HL reconstitution corresponding with pressure- and focal depth-dependent fluorescence microscopy imaging. This material is available free of charge via the Internet at http://pubs.acs.org.

■ AUTHOR INFORMATION

Corresponding Author
harrisj@chem.utah.edu; white@chem.utah.edu

■ ACKNOWLEDGMENT

This work was supported by the Defense Advanced Research Project Agency (FA9550-06-C-00C) and the National Science Foundation (CHE-0957242 and CHE-0616505).

■ REFERENCES

(1) Terstappen, G. C. *Drug Discov. Today* **2005**, *2*, 133–140.
(2) Dabraoski, M. A.; Dekermendjian, K.; Lund, P.-E.; Krupp, J. J.; Sinclair, J.; Larsson, O. *CNS Neurol. Disord.: Drug Targets* **2008**, *7*, 122–128.
(3) Haddock, P. *Am. Pharm. Rev.* **2006**, *9*, 119–122.
(4) Landry, Y.; Gies, J.-P. *Fundam. Clin. Pharmacol.* **2008**, *22*, 1–18.
(5) Jean-Yves, Le G.; Olivier, S.; Pierre, B.; Ahmed, A.; Christophe, V. *Recent Pat. Anti-Cancer Drug Discovery* **2007**, *2*, 189–202.
(6) Shim, J. W.; Gu, L. Q. *Anal. Chem.* **2007**, *79*, 2207–2213.
(7) Gu, L.-Q.; Braha, O.; Conlan, S.; Cheley, S.; Baley, H. *Nature* **1999**, *398*, 686–690.
(8) Bayley, H.; Braha, O.; Gu, L.-Q. *Adv. Mater.* **2000**, *12*, 139–142.
(9) Braha, O.; Gu, L.-Q.; Zhou, L.; Xiaofeng, L.; Cheley, S.; Bayley, H. *Nat. Biotechnol.* **2000**, *18*, 1005–1007.
(10) Deamer, D.; Branton, D. *Acc. Chem. Res.* **2002**, *35*, 817–825.
(11) Vercoutere, W. A.; Winters-Hilt, S.; DeGuzman, V. S.; Deamer, D.; Ridino, S. E.; Rodgers, J. T.; Olsen, H. E.; Marziali, A.; Akeson, M. *Nucleic Acids Res.* **2003**, *31*, 1311–1318.
(12) DeGuzman, V. S.; Lee, C. C.; Deamer, D. W.; Vercoutere, A. *Nucleic Acids Res.* **2006**, *34*, 6425–6437.
(13) Kasianowicz, J. J.; Brandin, E.; Branton, D.; Deamer, D. W. *Proc. Natl. Acad. Sci. U.S.A.* **1996**, *93*, 13770–13773.
(14) Akeson, M.; Branton, D.; Kasianowicz, J. J.; Brandin, E.; Deamer, D. W. *Biophys. J.* **1999**, *77*, 3227–3233.
(15) Meller, A.; Nivon, L.; Brandin, E.; Golovchenko, J.; Branton, D. *Proc. Natl. Acad. Sci. U.S.A.* **2000**, *97*, 1079–1084.
(16) Zhang, B.; Zhang, Y.; White, H. S. *Anal. Chem.* **2004**, *76*, 6229–6238.
(17) Zhang, B.; Zhang, Y.; White, H. S. *Anal. Chem.* **2006**, *78*, 477–483.
(18) Zhang, B.; Galusha, J.; Shiozawa, P. G.; Wang, G.; Bergren, A. J.; Jones, R. M.; White, R. J.; Ervin, E. N.; Cauley, C. C.; White, H. S. *Anal. Chem.* **2007**, *79*, 4778–4787.
(19) White, R. J.; Zhang, B.; Daniel, S.; Tang, J. M.; Ervin, E. N.; Cremer, P. S.; White, H. S. *Langmuir* **2006**, *22*, 10777–10783.
(20) White, R. J.; Ervin, E. N.; Yang, T.; Chen, X.; Daniel, S.; Cremer, P. S.; White, H. S. *J. Am. Chem. Soc.* **2007**, *129*, 11766–11775.
(21) Schibel, A. E. P.; Edwards, T.; Kawano, R.; Lan, W.; White, H. S. *Anal. Chem.* **2010**, *82*, 7259–7266.
(22) (a) Kawano, R.; Schibel, A. E. P.; Cauley, C.; White, H. S. *Langmuir* **2008**, *25*, 2850–2855. (b) Ervin, E. N.; Kawano, R.; White, R. J.; White, H. S. *Anal. Chem.* **2008**, *80*, 2069–2076. (c) Ervin, E. N.; Kawano, R.; White, R. J.; White, H. S. *Anal. Chem.* **2008**, *81*, 533–537. (d) Lathrop, D. K.; Ervin, E. N.; Barrall, G. A.; Keehan, M. G.; Kawano, R.; Krupka, M. A.; White, H. S.; Hibbs, A. H. *J. Am. Chem. Soc.* **2010**, *132*, 1878–1885. (e) Schibel, A. E. P.; An, N.; Jin, Q.; Fleming, A. M.; Burrows, C. J.; White, H. S. *J. Am. Chem. Soc.* **2010**, *132*, 17992–17995. (f) Chen, Q.; Liu, J.; Schibel, A. E. P.; White, H. S.; Wu, C. *Macromolecules* **2010**, *43*, 10594–10599.
(23) Bayley, H.; Cremer, P. S. *Nature* **2001**, *413*, 226–230.
(24) Mueller, P.; Rudin, D. O.; Tien, H. T.; Wescott, W. C. *J. Phys. Chem.* **1963**, *67*, 534–535.
(25) Tien, H. T.; Diana, A. L. *Chem. Phys. Lipids* **1968**, *2*, 55–101.
(26) White, S. H. *Biophys. J.* **1970**, *10*, 1127–1148.
(27) White, S. H. *Biophys. J.* **1972**, *12*, 432–445.
(28) White, S. H. . In *Ion Channel Reconstitution*; Miller, C., Ed.; Plenum Publishing Co.: New York, 1986, pp 3−35.
(29) Thompson, N. L.; Plamer, A. G., III; Wright, L. L.; Scarborough, P. E. *Comments Mol. Cell Biol.* **1988**, *5*, 109–131.
(30) Korlach, J.; Schwille, P.; Webb, W. W.; Feigenson, G. W. *Proc. Natl. Acad. Sci. U.S.A.* **1999**, *96*, 8461–8466.
(31) Samsonov, A. V.; Mihalyov, I.; Cohen, F. S. *Biophys. J.* **2001**, *81*, 1466–1500.
(32) Ide, T.; Yanagida, T. *Biochem. Biophys. Res. Commun.* **1999**, *265*, 595–599.
(33) Ries, R. S.; Choi, H.; Blunck, R.; Bezanilla, F.; Heath, J. R. *J. Phys. Chem. B* **2004**, *108*, 16040–16049.
(34) Suzuki, H.; Tabata, K. V.; Noji, H.; Takeuchi, S. *Langmuir* **2006**, *22*, 1937–1942.
(35) Sakmann, B., Neher, E., Eds. *Single-Channel Recording*; Plenum Press: New York, 1983.
(36) Hou, Y.; Bardo, A. M.; Martinez, C.; Higgins, D. A. *J. Phys. Chem. B* **2000**, *104*, 212–219.
(37) Martin-Brown, S. A.; Fu, Y.; Saroja, G.; Collinson, M. M.; Higgins, D. A. *Anal. Chem.* **2005**, *77*, 486–494.
(38) Krishnamoorthy, I.; Krishnamoorthy, G. *Biochim. Biophys. Acta* **1998**, *1414*, 255–259.
(39) Gao, G.; Mei, E.; Lim, M.; Hochstrasser, R. M. *J. Am. Chem. Soc.* **2006**, *128*, 4814–4822.
(40) Sackett, D. L.; Knutson, J. R.; Wolff, J. *J. Biol. Chem.* **1990**, *265*, 14899–14906.
(41) Dutta, A. K.; Kamada, K.; Ohta, K. *J. Photochem. Photobiol., A* **1996**, *93*, 57–64.
(42) Hou, Y.; Bardo, A. M.; Martinez, C.; Higgins, D. A. *J. Phys. Chem. B* **2000**, *104*, 212–219.
(43) Gao, F.; Mei, E.; Lim, M.; Hochstrasser, R. M. *J. Am. Chem. Soc.* **2006**, *128*, 4814–4822.
(44) Neher, E. *Biochim. Biophys. Acta* **1974**, *373*, 327–336.
(45) Fisher, L. R.; Parker, N. S. *Biophys. J.* **1984**, *46*, 253–258.
(46) Vassilev, P. M.; Kanazirska, M. P.; Tien, H. T. *Bioelectrochem. Bioenerg.* **1986**, *15*, 395–406.
(47) Mayer, M.; Kriebel, J. K.; Tosteson, M. T.; Whiteside, G. M. *Biophys. J.* **2003**, *85*, 2684–2695.